

# Scaling of the conductance in gold nanotubes

Miriam del Valle,<sup>1,2</sup> Carlos Tejedor,<sup>1</sup> and Gianaurelio Cuniberti<sup>2</sup>

<sup>1</sup>*Departamento de Física Teórica de la Materia Condensada,*

*Universidad Autónoma de Madrid, Facultad de Ciencias, C-V, E-28049 Madrid, Spain*

<sup>2</sup>*Institute for Theoretical Physics, University of Regensburg, D-93040 Regensburg, Germany*

(Dated: January 17, 2006)

A new form of gold nanobridges has been recently observed in ultrahigh-vacuum experiments, where the gold atoms rearrange to build helical nanotubes, akin in some respects to carbon nanotubes. The good reproducibility of these wires and their unexpected stability will allow for conductance measurements and make them promising candidates for future applications. We present here a study of the transport properties of these nanotubes in order to understand the role of chirality and of the different orbitals in quantum transport observables. The conductance per atomic row shows a light decreasing trend as the diameter grows, which is also shown through an analytical formula based on a one-orbital model.

PACS numbers:

Gold is known to be a good conductor for ages but its use in nanoelectronics delivers unexpected behaviors differing from its bulk properties. Recent experiments<sup>1,2,3</sup> indicate that gold nanowires exhibit fascinating ordered structures that resemble those of the by now well-known carbon nanotubes (CNTs).<sup>4</sup>

High resolution microscope images show that these wires consist of coaxial nanotubes of helical atom rows coiled around the wire axis. These wires present therefore different possible helicities as CNTs do, depending on the angle in which the atom rows rotate around the tube axis. Experimental evidence so far seems to support the fact that small chiral angles are preferred by the fabricated nanotubes. The multi-shell nanotubes keep the difference in the number of atom rows between adjacent shells constant, leading to a kind of magic shell-closing number which is always seven. This fact can be understood as a new inner shell arises when the radii differ in about  $a = 2.88 \text{ \AA}$ , the neighboring distance of bulk gold, which implies a perimeter difference ( $2\pi a \sim 7a$ ) corresponding to seven atom rows nearly parallel to each other. So single-walled nanotubes should exist with six or less atom rows, and actually one single-walled tube with five atom rows has been observed.<sup>3</sup> With seven or more atom rows a double-walled tube should be seen, which becomes a triple-walled nanotube when more than fourteen rows are present, and so on. The good reproducibility of these wires, and their stability,<sup>5,6,7,8</sup> which is better for those with outer tubes with an odd number of atom rows, makes them promising candidates for future applications. Ballistic conductance measurements will lead to a confirmation of the proposed structural model through its derived electronic structure. Astonishingly enough several works hint at the fact that the conductance per atom row might decrease with the number of circumferential atoms.<sup>9,10</sup> In this Letter, we provide a theoretical understanding of this phenomenon by means of both numerical and analytical calculations.

Determining the structure of the nanotubes is fundamental in order to understand their physical properties,

such as conductance quantization. Experimental evidence points out that a structural transition from the thicker, internally crystalline wires into these thinner regular but noncrystalline ones takes place at a critical radius below 2 nm. Lattice spacing has been measured to be almost 2.88 Å, the neighboring distance of gold, for all these wires with diameters between 0.5 nm and 1.5 nm. We therefore take this distance as the interatomic spacing of the triangular lattice, as we can think of these cylindrical tubes as rolled-up lattice planes of fcc Au (111), as depicted in Fig. 1. Atoms in successive shells appear to strain a bit to maintain commensurability between inner and outer shells. Ab-initio calculations show though that this shear strain should have just a very small effect on

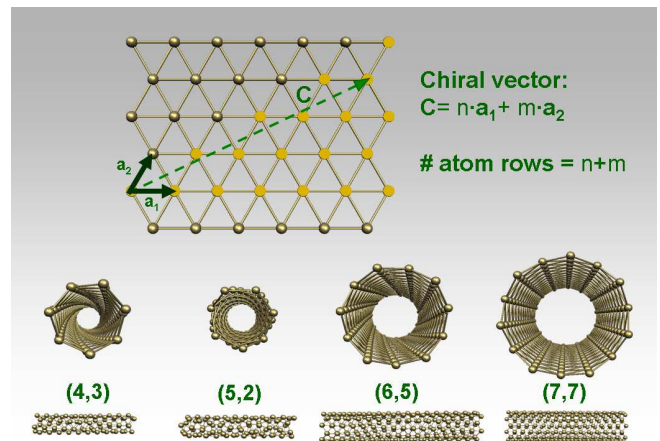


FIG. 1: Some gold nanotubes are shown as well as the 2D triangular network, from which we can build these models. The coordinate system used is sketched on the lattice, being  $\mathbf{a}_1$  and  $\mathbf{a}_2$  the basis vectors, and  $\mathbf{C}$  the chiral vector specifying the nanotube and corresponding to its circumference. The highlighted atoms on the lattice are those defining the region of inequivalent chiral vectors, which spans an angle of  $30^\circ$  as can be easily understood analyzing the symmetry of the lattice.

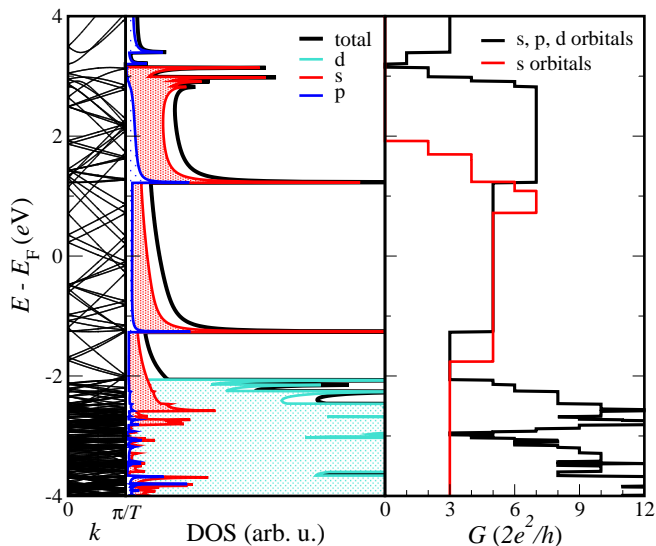


FIG. 2: Onedimensional band structure, density of states and conductance for the (4,3) gold nanotube. For this tube the translational vector is  $T = |\mathbf{T}| = 3.03$  nm. The energies are shifted to set the origin at the Fermi energy, as in the next figures.

the electronic structure.<sup>11</sup>

Despite the strong intershell interactions, these structures resemble greatly those of CNTs, where the honeycomb network of carbon atoms is replaced by the triangular lattice of gold atoms. These are actually complementary networks, and the gold nanotube structure can be obtained from the one of CNTs by putting gold atoms at the center of honeycomb framework.

We use the indices  $(n, m)$  to classify the gold nanotubes (AuNTs), where  $n$  and  $m$  are integers defining the chiral vector, which is wrapped to form the tube. The chiral vector is then  $(n\mathbf{a}_1 + m\mathbf{a}_2)$ , perpendicular to the tube axis, where the vectors  $\mathbf{a}_1$  and  $\mathbf{a}_2$  span the 2D unit cell. The number of atom rows coiling around the tube axis is then  $n + m$  while the nanotube translational vector reads  $\mathbf{T}(n, m) = ((2m + n)/d_R)\mathbf{a}_1 - ((2n + m)/d_R)\mathbf{a}_2$ , being  $d_R$  the greatest common divisor of  $(2m + n)$  and  $(2n + m)$ , as  $\mathbf{T}$  should be the smallest lattice vector in its direction. Due to the symmetry of the triangular lattice the chiral vectors of all inequivalent tubes are comprised in a  $30^\circ$  angle, that is, in a one-twelfth irreducible wedge of the Bravais lattice. We can then compromised and use only indices with  $n > 0$  and  $0 < m < n$ . The tubes of the form  $(n, 0)$  and  $(n, n)$  are achiral, presenting thus no handedness. Only wires with an even number of strands may have the structure  $(n, n)$ .<sup>12</sup>

For a fixed  $n$ , the radius is minimized for higher values of  $m$  (tension decreases with shrinking radius), so as to fulfill simultaneously tightest external packing and minimal wire radius.<sup>8</sup> The largest  $m$  for odd number of atom rows is  $n - 1$ , leading always to a finite chirality and thus a helical structure in these cases. The outer tubes with an even number of atom rows seem to take non-helical

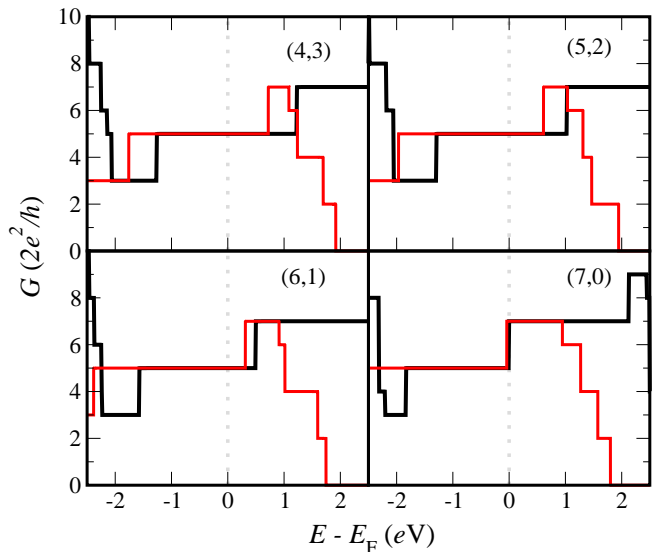


FIG. 3: Conductance of AuNTs with seven atom rows but different chiralities. Red lines indicate results including  $s$  orbitals only, whereas the black ones are showing the calculations with all nine outer orbitals.

structures with shorter periods. The helicity of the tubes is observed experimentally through a wavy modulation of the STM images.<sup>2,3</sup>

We study the transport properties of several of these AuNTs using a multiorbital tight-binding Hamiltonian and Green function techniques. In particular we adopt a Slater-Koster-type<sup>13</sup> tight-binding approach, with the parameters taken from the nonorthogonal parametrization of Papaconstantopoulos and co-workers.<sup>14</sup> Our approach remains of microscopic nature since the symmetries of the atomic  $s, p$ , and  $d$  valence orbitals are taken into account. Ab initio studies including shell effects could be needed for greater quantitative accuracy.

As a result we analyze the differences in the transport calculations that raise from the inclusion of all outer  $s, p$  and  $d$  orbitals instead of just the simplified model of  $s$  orbitals, which is a tempting approximation for these kind of systems and has been used in other works.<sup>9</sup> In order to compare results, we will thus use both a one-orbital Hamiltonian describing just the  $s$  orbitals, and a nine-orbital Hamiltonian, containing  $s, p$  and  $d$  orbitals including all conduction electrons. In doing that we restrict our calculations to nearest-neighbors interactions. The Hamiltonian describing our systems can be written as

$$\mathcal{H} = \sum_{\langle i, j \rangle, \alpha, \beta} H_{i\alpha, j\beta} c_{i\alpha}^\dagger c_{j\beta} \quad (1)$$

where the indices  $i, j$  run over the atom sites and the indices  $\alpha, \beta$  mark the different orbitals. The transfer integrals  $H_{i\alpha, j\beta}$  are the on-site energies or hopping parameters, dependent on whether  $i$  equals  $j$  or not.

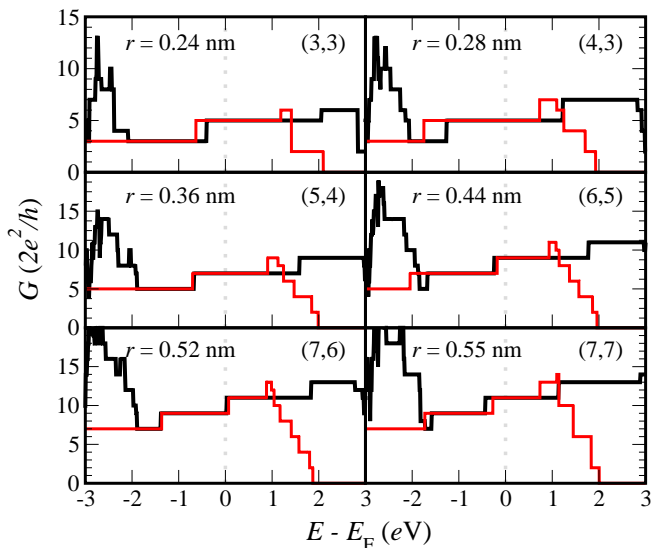


FIG. 4: Conductance of AuNTs with different radii  $r$ . Red lines indicate results including  $s$  orbitals only, whereas the black ones are showing the calculations with all nine outer orbitals.

The conductance is calculated from the transmission values applying the Landauer formula, using Green function techniques.<sup>15</sup> In particular, we derive the elastic linear response conductance via the Fisher-Lee formula for the quantum mechanical transmission<sup>16</sup>:  $G = \frac{2e^2}{h} \text{Tr} \{ \Gamma_L \mathcal{G} \Gamma_R \mathcal{G}^\dagger \}$ , where  $\Gamma_{L/R} = i \left( \Sigma_{L/R} - \Sigma_{L/R}^\dagger \right)$  being  $\Sigma_{L/R}$  the self energy of the left or right lead respectively, and where  $\mathcal{G}$  is the Green function of the central region dressed by the electrodes.

We consider semi-infinite single-walled nanotubes (SWNTs) as leads. Considering the leads as bulk gold will yield an increased imaginary part of the lead self energies, which will slightly decrease the conductance values. For multi-walled nanotubes (MWNTs) it has been suggested that the conductance  $G$  is mainly determined by the outer shell which is also responsible for the structural stability.<sup>17</sup> A slight reduction of the conductance is expected from the finite size effects.

The calculated density of states and the conductance for the gold nanotube (4,3) are shown in Fig. 2. This tube is one of the simplest possible candidates with seven atom rows around its circumference (Fig. 1). The colored areas show the contribution of the different orbitals to the total density of states, indicating a dominance of  $s$  orbitals around the Fermi level. Considering only  $s$  orbitals around the Fermi energy is thus a good approximation, but when applying a bias it can be critical to include all  $s, p, d$  outer orbitals, as they play an important role in the opening of new conduction channels.

A comparison of the conductance of nanotubes of the same diameter but different chiralities, as shown in Fig. 3, suggests that no significant difference is expected in their conductance values at the Fermi energy. For applied bias

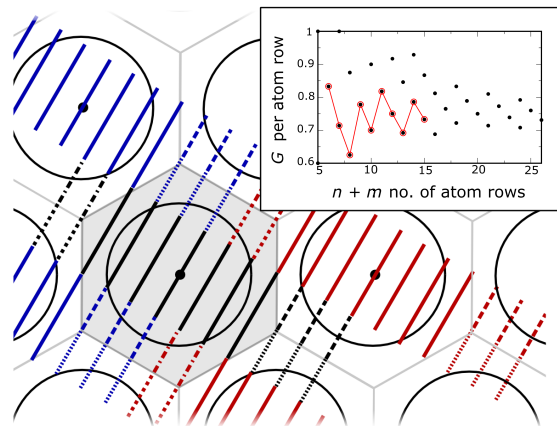


FIG. 5: Schematic illustration of the reciprocal lattice of the 2D hexagonal Bravais lattice of Au (111) where the first Brillouin zone is highlighted through a darker background. The  $k$ -vectors lying at the Fermi surface give rise to a nearly perfect circle in this 2D structure. The black cutting lines represent the Brillouin zone of a nanotube in an extended zone scheme which allows the use of the dispersion relation calculated for the 2D gold layer to get the bands of a folded nanotube. In this example we show the wave vectors giving the bands in a (6,0) AuNT, a good candidate for this visualization as it has a small number of bands. These lines are plotted as solid bands inside the first Brillouin zone, and colored when folded back into it through the reciprocal lattice vectors of the gold layer. In the inset the conductance per atom row at the Fermi energy based on the analytical model accounting only for  $s$ -orbitals described in this Letter is shown for all possible  $(n,m)$  NTs, reproducing exactly the values of the numerical calculations.

voltages the current will show the difference in energies at which new channels start taking part in transport.

In Fig. 4 the conductance is plotted for nanotubes of different radii, chosen as to have the smallest chirality possible for a given radius. The number of atom rows around the nanotube axis in each of them is 6, 7, 9, 11, 13 and 14 respectively. We see that, though the conductance increases for thicker nanotubes, this is not the general trend if divided by the number of atom rows. We can observe again how the expansion of the orbital basis to include all conduction electrons changes the energies at which new channels open, being critical to obtain correct current values.

By analyzing the Brillouin zone of the two-dimensional gold lattice taking into account only  $s$  orbitals, one can easily demonstrate after studying its dispersion relation that the Fermi surface is with great accuracy approximated by a circle with a radius close to  $k_F = 2\sqrt{\pi}/(\sqrt[4]{3}a)$ , where  $a = 2.88 \text{ \AA}$ . This simple model allows us to have an analytical approach to the conductance, as the number of energy bands crossing the Fermi surface, since the Brillouin zone of the gold nanotubes consist of parallel line segments due to the quantization of the wave vector along the circumferential direction. For simplicity

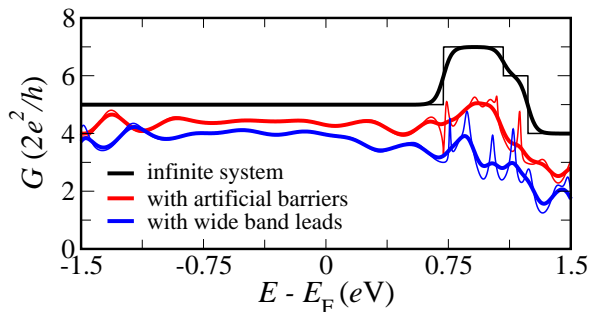


FIG. 6: Conductance of the (4,3)-AuNT for a perfect infinite NT (black line), for a finite tube with barriers in the connecting regions to the electrodes (where the constant  $\alpha$  introduced in the text equals 0.6) and for a finite tube like in the previous case but in the wide band limit approximation taken at the Fermi energy. The colored lines show oscillations due to scattering at the ends of the finite size tube. The thicker lines correspond to room temperature conductance.<sup>19</sup>

we can restrict this counting to the first Brillouin zone by folding back to this area the segments lying outside it, which will elongate the lines inside it, as pictured in Fig. 5.<sup>18</sup> The conductance can then be written as

$$G = \frac{2e^2}{h} \left[ 2 \text{Int} \left( \sqrt{\frac{n^2 + m^2 + nm}{\pi\sqrt{3}}} \right) + 1 \right] \quad (2)$$

and is only dependent of the nanotube indices and not on hopping parameters or on-site energies. This models yields a perfect matching with the numerical calculations described before. The result of this approximation of the conductance at the Fermi level is plotted in the inset of Fig. 5 for nanotubes of different radii and chiralities, presenting the conductance per atom row. The solid lines in this figure put an accent on the results of AuNTs with the smallest helicity as characterized in Fig. 4. We can observe how the envelope of all these points slowly decreases with increasing number of coiling atom rows, or likewise with increasing diameter. The conductance values will nevertheless be reduced by considering more realistic gold leads. This trend has been also found in a first-principles one-orbital calculation.<sup>9</sup>

Gold nanotubes have been observed as short ( $L \sim 4$  nm) conductors between bulk gold electrodes. This calls for an extension of our theory to account for finite size effects. We did this by parametrically introducing into the nanotube two tunneling barriers at a distance  $L$ . Fig. 6 shows the conductance between two homologous semi-infinite electrodes which are taken into account through modified self energies. This modification is introduced by a multiplicative factor  $\alpha$ , which simulates the barriers. The finite size effects can be equally made apparent by considering wide band leads, *i.e.*  $\Sigma_{WB}(E) \cong -i \text{Im}\Sigma(E = E_F)$ . As we can see in Fig. 6, we obtain the same kind of oscillating behavior with both approximations. This shows that the results of our model provide an upper limit for the conductance.

In conclusion, we investigated the electronic properties of several gold nanotubes. We built the Hamiltonians of the systems by applying a tight-binding model for  $s$  orbitals as well as for all outer orbitals. All AuNTs are equally metallic independently of their chirality or diameter in contrast to the results obtained for their carbon counterparts,<sup>20</sup> but expected from gold electronic nature. In the case of gold the quantization of electron waves along the circumference of the tube results in a Brillouin zone composed of line segments that always cut the Fermi surface of the Au [111] layer due to the continuity of this surface. The  $s$ -orbital calculations demonstrate that a one-orbital approach to the problem of gold nanotubes is not a bad approximation, but should be avoided when applying a finite bias voltage to the system.

An analytical formula for the conductance of the  $s$ -orbital calculations, matching perfectly the numerical results, shows that there is a slight decrease of the conductance per atom row as the radius increases.

### Acknowledgments

This work was partially funded by the Volkswagen Foundation (Germany) under grant No. I/78 340, by the MEC (Spain) under contracts MAT2005-01388, NAN2004-09109-CO4-04, and by the CAM under contract No. S-0505/ESP-0200. MD acknowledges the support from the FPI Program of the Comunidad Autónoma de Madrid.

<sup>1</sup> Y. Kondo and K. Takayanagi, Phys. Rev. Lett. **79**, 3455 (1997).

<sup>2</sup> Y. Kondo and K. Takayanagi, Science **289**, 606 (2000).

<sup>3</sup> Y. Oshima, A. Onga, and K. Takayanagi, Phys. Rev. Lett. **91**, 205503 (2003).

<sup>4</sup> S. Reich, C. Thomsen, and J. Maultzsch, *Carbon Nanotubes* (Wiley-VCH, Berlin, 2004), ISBN 3-527-40386-8; R. Saito, G. Dresselhaus, and M. S. Dresselhaus, *Physical Properties of Carbon Nanotubes* (Imperial College Press, London, 1998), ISBN 1-86094-093-5; E. Thune and C. Strunk, *Introducing Molecular Electronics* (Springer,

Berlin and Heidelberg, 2005), chap. 13.

<sup>5</sup> O. Gülseren, F. Ercolessi, and E. Tosatti, Phys. Rev. Lett. **80**, 3775 (1998).

<sup>6</sup> G. Bilalbegović, Phys. Rev. B **58**, 15412 (1998).

<sup>7</sup> E. Z. da Silva, A. J. R. da Silva, and A. Fazzio, Phys. Rev. Lett. **87**, 256102 (2001).

<sup>8</sup> E. Tosatti, S. Prestipino, S. Kostlmeier, A. D. Corso, and F. D. Tolla, Science **291**, 288 (2001).

<sup>9</sup> T. Ono and K. Hirose, Phys. Rev. Lett. **94**, 206806 (2005).

<sup>10</sup> R. T. Senger, S. Dag, and S. Ciraci, Phys. Rev. Lett. **93**, 196807 (2004).

- <sup>11</sup> X. Yang and J. Dong, Phys. Rev. B **71**, 233403 (2005); C.-K. Yang, Appl. Phys. Lett. **85**, 2923 (2004).
- <sup>12</sup> We can decode our notation  $(n, m)$  into the one used in parallel with lattice vectors spanning an angle of  $120^\circ$  like  $(n + m, n)$  for an equivalent AuNT for transport.
- <sup>13</sup> J. C. Slater and G. F. Koster, Phys. Rev. **94**, 1498 (1954).
- <sup>14</sup> D. A. Papaconstantopoulos, *Handbook of the Band Structure of Elemental Solids* (Plenum, New York, 1986).
- <sup>15</sup> G. Cuniberti, F. Grossmann, and R. Gutiérrez, Advances in Solid State Physics **42**, 133 (2002).
- <sup>16</sup> D. S. Fisher and P. A. Lee, Phys. Rev. B **23**, 6851 (1981).
- <sup>17</sup> A. Hasegawa, K. Yoshizawa, and K. Hirao, Chem. Phys. Lett. **345**, 367 (2001).
- <sup>18</sup> W. A. Harrison, Phys. Rev. **118**, 1190 (1960).
- <sup>19</sup> P. F. Bagwell and T. P. Orlando, Phys. Rev. B **40**, 1456 (1989).
- <sup>20</sup> R. Saito, M. Fujita, G. Dresselhaus, and M. Dresselhaus, Appl. Phys. Lett. **60**, 2204 (1992); N. Hamada, S. Sawada, and A. Oshiyama, Phys. Rev. Lett. **68**, 1579 (1992).